

Combined effects of wind, air temperature and snowfall on snow accumulation in a subalpine forest

Alex Cebulski & John Pomeroy

April 30, 2024

TODO

look at wind flow in canopy equations:

- Cionco (1972)
- Zhu et al. (2001)
- parvanians, ellis, JM thesis

Introduction

Forest cover extends over approximately half of North America's snow-covered region, governing snowpack accumulation and ablation, thereby influencing the timing and magnitude of runoff generation from snowmelt.

- There is a need for robust models of snow redistribution by vegetation and wind to estimate snow accumulation in mountain forests. To achieve this, a comprehensive understanding of snow redistribution processes is required. However, existing snow interception parameterizations are based on limited observations in distinct climates and forest structures. Rapid changes in climate and forest ecology illustrate the pressing need to assess whether existing snow interception parameterizations are suitable for predicting snow accumulation in diverse and changing environments.
- Intercepted snow in the canopy is subjected to higher rates of sublimation compared to subcanopy snow due to greater surface area, higher wind speed, and solar exposure (Pomeroy et al., 1998). Across the Northern Hemisphere, researchers estimate that 25 to 45% of annual snowfall may be lost to the sublimation of intercepted snow from the canopy (Essery et al., 2003). Correctly determining the fraction of snowfall intercepted

in the canopy is crucial for estimating interception losses by sublimation (Pomeroy et al., 1998). In addition, the time that snow resides in the canopy and is subject to sublimation is dependent on rates of unloading, melt, drip, and resuspension of snow (Hedstrom & Pomeroy, 1998; Katsushima et al., 2023; Lumbrazo et al., 2022; Storck et al., 2002).

- The theory underpinning current snow interception parameterizations is based on observations ranging from warm maritime (Andreadis et al., 2009; Storck et al., 2002) and cold continental (Ellis et al., 2010; Hedstrom & Pomeroy, 1998; Roesch et al., 2001; Satterlund & Haupt, 1967) climates generally characterized by dense forest canopy. Accurate simulations of forest snow accumulation have been achieved if the parameterizations are applied in similar climates to where they were developed (Lundquist et al., 2021; Rasouli et al., 2019; Roth & Nolin, 2019) or if they are combined into a hybrid parameterization and assessed at global and regional scales in a wide range of climates (Essery et al., 2003; Gelfan et al., 2004). Although accurate performance has been achieved across different climates in some studies (Essery & Pomeroy, 2004; Gelfan et al., 2004), other snow model comparisons (Krinner et al., 2018; Rutter et al., 2009) have shown reduced performance. The decision in earth system models to use parameterizations derived in warm or cold climates is often based on a simple temperature-based step function (Essery et al., 2003; Gelfan et al., 2004) and may require modification to better represent more transitional climates and forest types. The original theory has also been simplified over time, i.e. the increase in canopy coverage with increasing wind speed is not included in more recent parameterizations Roth & Nolin (2019). Updates by Gelfan et al. (2004) to combine the Hedstrom & Pomeroy (1998) and Storck et al. (2002) parameterizations is not typically utilized in recent studies (Krinner et al., 2018; Rutter et al., 2009). The omission or simplified representation of processes and reliance on empirical calibrations likely contribute to model uncertainty when applied in climates and forests where other processes become important (Krinner et al., 2018; Lumbrazo et al., 2022; Lundquist et al., 2021; Moeser et al., 2015; Roth & Nolin, 2019; Rutter et al., 2009).
- Figure 1 shows the difference in the change in interception efficiency across different snowfall event sizes for three common models. Interception efficiency (interception/snowfall) declines with increasing snow load (Hedstrom & Pomeroy, 1998; Storck et al., 2002) or initially increases and then is followed by a decline (Moeser et al., 2015). The underlying theory of the Moeser et al. (2015) parameterization stems from the Satterlund & Haupt (1967) study who observed an initial increase in the rate of intercepted snow, as snowflakes bridge gaps between needles. It may also be inferred that during the small near 0°C snowfall events observed in Satterlund & Haupt (1967) the majority of snow may have melted immediately due to a warm canopy resulting in low interception efficiency. The initial low interception efficiency was followed by an increase and then flattening off of the interception rate as branches bend due to the weight of snow which Satterlund & Haupt (1967) represented by a numerical analytical sigmoidal function. In the observations by Hedstrom & Pomeroy (1998), snow interception efficiency starts high and then declines. Hedstrom & Pomeroy (1998) hypothesis the shape of this curve is due to a decrease in canopy contact area and change in the incoming snowfall angle

of impact as branches bend downward. This relationship was best represented using an inverse exponential function shown in Figure 1. The Hedstrom & Pomeroy (1998) parameterization therefore differs from the (Moeser et al., 2015; Satterlund & Haupt, 1967) sigmoidal function as it does not include a representation for the initially slow interception rate. Andreadis et al. (2009) developed a snow interception model using data collected by Storck et al. (2002) in dense old growth forest in the maritime climate of southwestern Oregon, USA. This method builds off the maximum canopy snow load theory proposed in Hedstrom & Pomeroy (1998) but makes additional modifications to include a step function based on temperature. Here, snow interception efficiency, was found equal to a constant of 0.6 based on snow interception observations from Storck et al. (2002) in southern Oregon.

- Maximum interception capacity decreases (Hedstrom & Pomeroy, 1998) or increases (Storck et al., 2002) with increasing air temperature (Figure 2). Hedstrom & Pomeroy (1998) proposed that fresh snow density, which may be described as a function of air temperature (Hedstrom & Pomeroy, 1998), plays an important role in governing the interception capacity. Storck et al. (2002) limit, L as being less than or equal to the maximum interception storage L_{max} using a step function of temperature based on observations of warmer snow having more cohesion to the canopy.
- More recent work by Katsushima et al. (2023) collected measurements of snow interception using a weighed tree for a warm-humid coastal environment in Japan. They observed a decline in interception efficiency with increasing wind speed, they attributed to increased hydrometeor velocity and bouncing on impact. While not mentioned in this study, the decrease in interception efficiency may also be due to wind induced unloading. They did not observe a maximum interception capacity within their measurement range of 0-25 mm. Although for temperatures above 0 they could see a decline in interception efficiency above 10 mm maybe due to branch bending + melt rates. Katsushima et al. (2023) suggest air temperature and wind speed alone are insufficient to describe interception efficiency and hypothesize that particle shape may be an improved predictor but did not have the observations to test this. Some of the limited model performance reported by Katsushima et al. (2023) may be attributed to a result of their interception measurements including unloading due to melt and wind.
- Previous studies have collected measurements of interception efficiency over snowfall events ranging from hourly (Storck et al., 2002) to weekly timesteps (Hedstrom & Pomeroy, 1998). The different measurement time intervals vary in the amount of time possible for ablative processes and may influence model estimates of interception. As a result, some of the interception measurements inevitably include some amount of ablation. Despite the inclusion of unloading in the interception parameterizations developed in these studies, they are often combined with additional unloading parameterization in earth system models (Clark et al., 2015; Ellis et al., 2013) leading to some potential of double counting of the ablation process.

- Uncertainties also arise in the scaling of point or branch scale measurements to the plot scale (Staines & Pomeroy, 2023).
- Forest structure governs the interception efficiency observed at a given location (Hedstrom & Pomeroy, 1998; Roth & Nolin, 2019). Metrics used in common snow interception parameterizations (Hedstrom & Pomeroy, 1998; Storck et al., 2002) to describe forest structure include canopy cover and leaf area index (LAI). Leaf area index is defined by Chen et al. (1997) as one half the total green leaf area per unit ground surface area. Canopy cover is defined in Hedstrom & Pomeroy (1998) as the fraction of sky not visible by the instrument from under the canopy. While more detailed forest structure metrics exist derived from detailed LiDAR scans (Helbig et al., 2020; Roth & Nolin, 2019), often they are not available at regional extents required to run hydrological models.
- Add sentence on Staines & Pomeroy (2023).
- Several processes govern the accumulation of snow in mountain forests, and the importance of individual processes may differ depending on climate and forest structure (Gelfan et al., 2004; Hedstrom & Pomeroy, 1998; Moeser et al., 2015; Staines & Pomeroy, 2023). Therefore determining the dominant processes in varying climate and forests structures is important to guide model decision makers on what existing model parameterizations to choose or if a hybrid approach may be appropriate.
- New observations of snow interception and ablation processes will help determine if existing theories are applicable in differing climates and diverse forest structures.
- The novelty of this study is the study site location in a windswept discontinuous subalpine ridge forest and the use of high temporal frequency automated measurements and discrete high spatial resolution measurements using aerial LiDAR to attempt to separate out interception from ablative processes. Timelapse cameras were also used to confirm absence of unloading during interception periods.
- Existing theory relies on the green smear approach or using LAI + CC which does not appropriately describe the heterogeneity of discontinuous canopies

Objective: To assess the influence of canopy structure and meteorology on snow interception processes in a windswept subalpine forest.

Research Questions:

1. Are the theories and assumptions of existing snow interception parameterizations true for field measurements collected in a continental subalpine forest?
2. What are the dominant processes that control snow interception in a subalpine forest?

Specific Questions

- Is meteorology important for governing I/P?

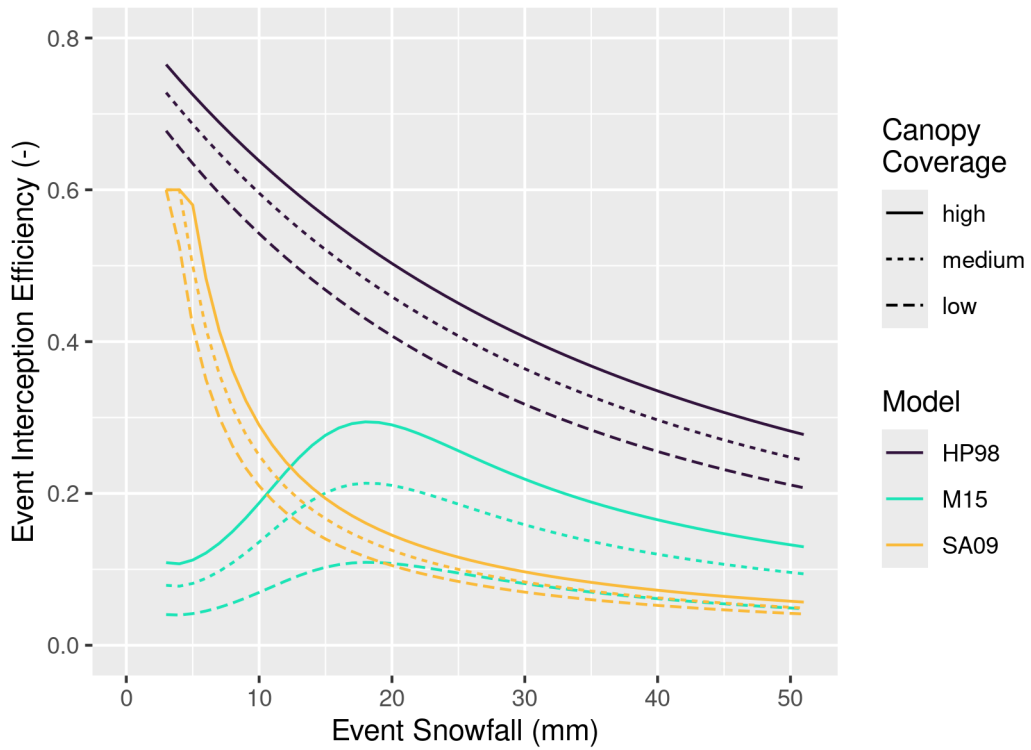


Figure 1: Example simulation of snow interception parameterizations by Hedstrom and Pomeroy (1998) (HP98), combined Storck et al. (2002) and Andreadis et al., (2009) (SA09), and the Moeser et al., (2009) (M15). Event interception efficiency is the change in canopy SWE storage divided by the corresponding change in SWE in the open. The temperature for the example events are held constant at -5 °C. The canopy coverage values are 0.75 (low), medium (0.80) and high (0.83).

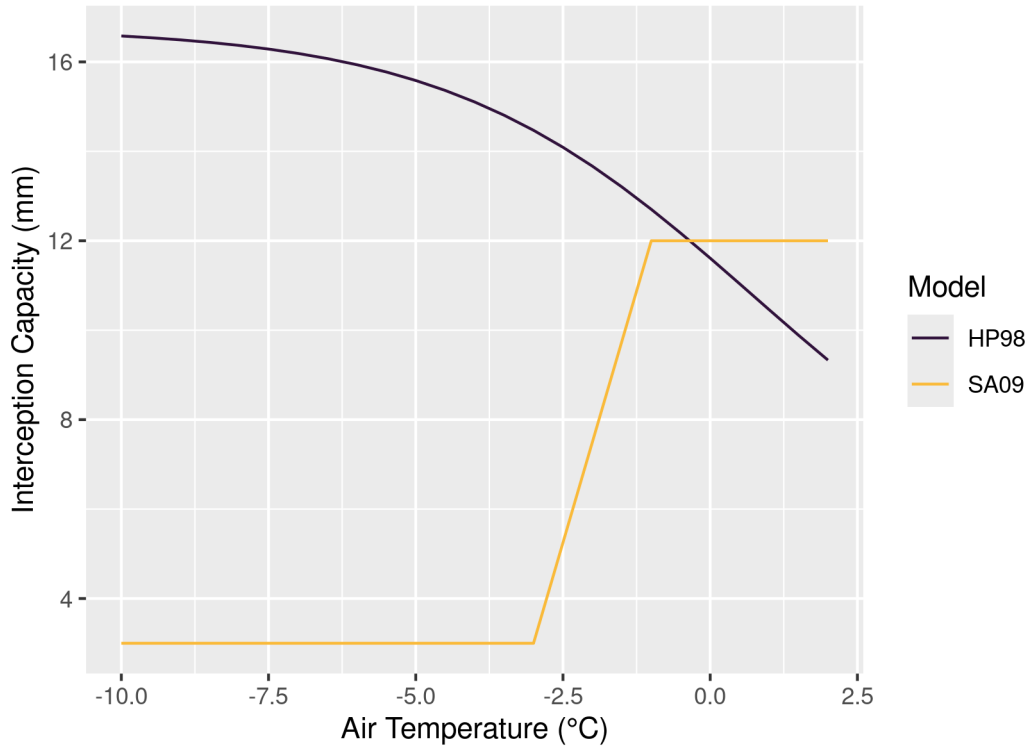


Figure 2: A comparison of the Hedstrom & Pomeroy (1998) (HP98) and Andreadis et al. (2009) (SA09) interception capacity parameterizations. Since the HP98 parameterization is a function of new snow density as a result the interception capacity is negatively related to air temperature.

- How does hydrometeor trajectory angle influence apparent canopy structure?
- How does the association between canopy structure and I/P vary across the hemisphere for an event with moderate wind speed?
- Is this association stronger when there is snow in the canopy i.e., branches have been bridged or reduced due to branch bending?

Theory

Figure 3 shows the mass exchange of snowfall between the forest canopy and the snowpack on the ground surface. The storage of snow water equivalent (SWE) is represented here with respect to the canopy (L , mm) or the surface snowpack (S , mm). Fluxes that are repeated between the canopy and snowpack control volume have a superscript to specify what control volume they refer to (i.e. q^{veg} refers to the vegetation control volume and q^{snow} refers to the surface snowpack control volume).

The change in canopy SWE storage, L (mm), may be represented as:

$$\frac{dL}{dt} = q_{sf} - q_{tf}(L) - q_{unld}(L) - q_{drip}(L) - q_{wind}^{veg}(L) - q_{sub}^{veg}(L) \quad (1)$$

where q_{sf} (mm s⁻¹) is the above canopy snowfall rate, q_{tf} (mm s⁻¹) is the throughfall rate, q_{wind}^{veg} (mm s⁻¹) is the wind transport rate in our out of the control volume (typically assumed to be negligible in the literature), q_{sub}^{veg} (mm s⁻¹) is the intercepted snow sublimation rate, q_{unld} (mm s⁻¹) is the canopy snow unloading rate and q_{drip} (mm s⁻¹) is the canopy snow drip rate due to canopy snowmelt. q_{wind}^{veg} and q_{sub}^{veg} may be a positive or negative flux. Where all of the above rates are a function of snow load (L), which is how much snow is present in the canopy.

Hedstrom & Pomeroy (1998) hypothesized that a change in hydrometeor trajectory angle was a factor in influencing interception efficiency. Figure 4 shows the theoretical increase in trajectory angle with increasing wind speed.

The trajectory angle, θ_h of a hydrometeor as the departure in degrees (°) from a horizontal plane (i.e., -90° for vertical snowfall), may be calculated as:

$$\theta_h = \arctan \left(\frac{-v_h(D_h)}{x_h(u_z)} \right) * \frac{180}{\pi} \quad (2)$$

where v_h is the terminal fall velocity of the hydrometeor (m s⁻¹), which is a function of the hydrometeor diameter, D_h , x_h is the horizontal change in the hydrometeor (m s⁻¹) which is a function within canopy wind speed, u_z at height above ground, z .

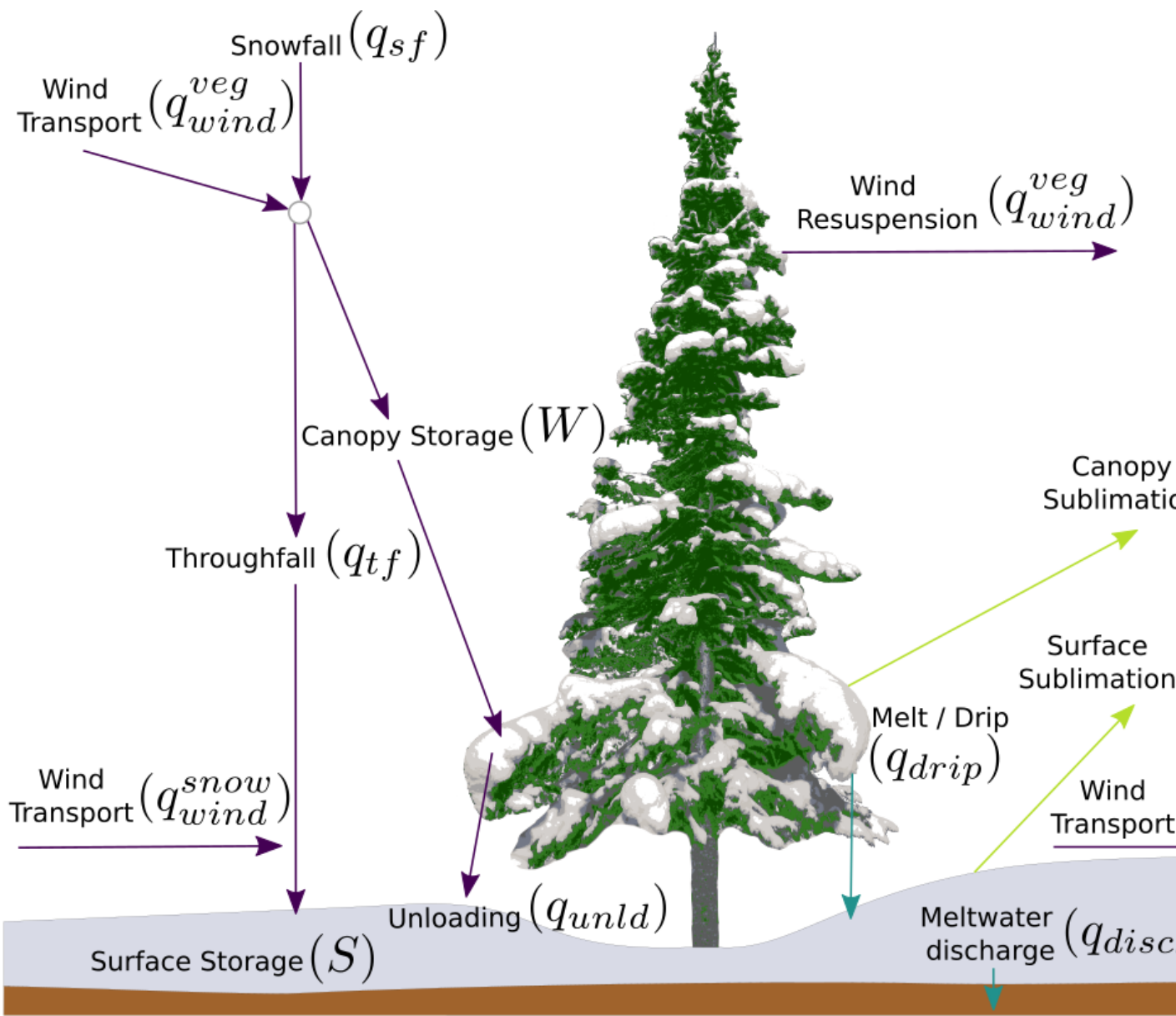


Figure 3: The mass balance of intercepted snow in a coniferous forest canopy and the sub-canopy snowpack. The colours of the arrows correspond to the water phase: solid (purple), liquid (blue) and vapour (light green). The head of the arrow indicates a positive flux either into the control volume (positive) or away from the control volume (negative). Note that the fluxes may transition between positive and negative. In the case of sublimation, from the canopy or snowpack, the flux may be positive (sublimation) or negative (deposition). This figure was adapted from Pomeroy and Gray, (1995).

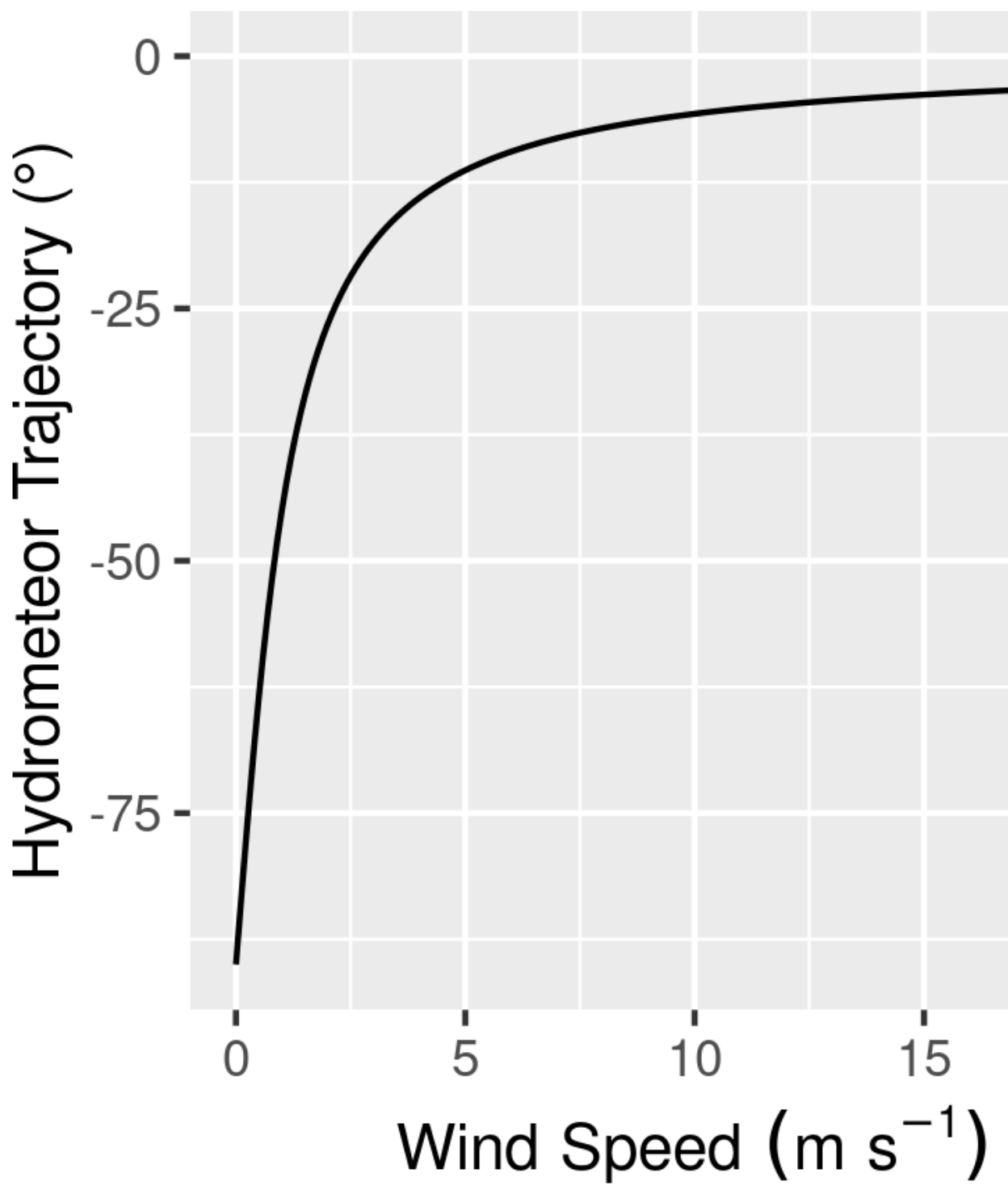


Figure 4: The theoretical relationship of hydrometeor trajectory (departure from horizontal plane) with increasing wind speed. This assumes a constant hydrometeor velocity of 1 m/s, typical of snowfall and a horizontal velocity equal to wind speed.

Above the top of the canopy, wind flow is approximately logarithmic with height. Cionco (1965) show that, u_z may be approximated using the exponential formula:

$$u_z = u(u^*, z, z_o, d) \cdot \exp \left[a \cdot \left(\frac{z_c}{h_c} - 1 \right) \right]$$

where u is the horizontal wind speed at the top of the canopy which is a function of the friction velocity u^* , height above ground, z , roughness length, z_o , and the displacement height of the canopy, d . a is an attenuation coefficient that increases with increasing leaf area and decreases as the mean distance between individual trees increases, z_c is the height above ground of u_z , and h_c is the average height of the canopy elements. Cionco (1972) suggest values for a of 1.01 for small needleleaf trees, Zhu et al. (2001) provide methods to calculate a based on canopy density and Parviaainen & Pomeroy (2000) provide a method to calculate a using observations from two jack pine (*Pinus banksiana*) stands.

Methods

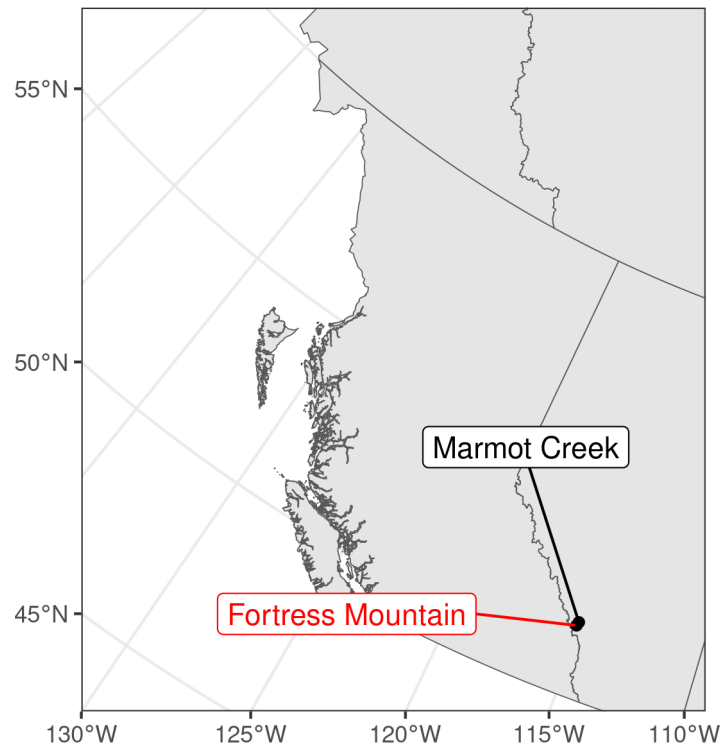
Study Site

This study was conducted at the Subalpine Ridge Forest (SRF) site located in the Fortress Mountain Research Basin (FMRB), AB ~ 51 ° N, 2100 m asl., a continental headwater basin with sparse subalpine forest (Figure 5a). In-situ observations of forest snow accumulation, snow interception, and canopy snow ablation were collected over the 2022 and 2023 water years. The species of trees at the SRF site is comprised of coexisting subalpine fir (*Abies lasiocarpa*) and Engelmann spruce (*Picea engelmannii*), with a proportion of 70% and 30% respectively (Langs et al., 2020). In the early 1900s the majority of the SRF vegetation burned during a large forest fire that affected most of the Kananaskis Valley. Following the fire, the forest has naturally regenerated with minimal disturbance.

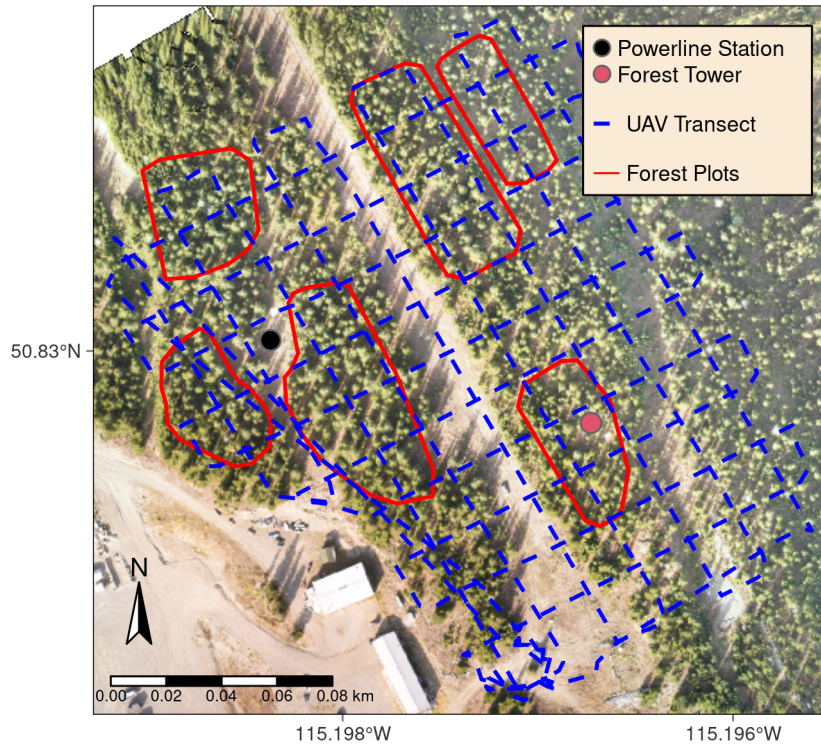
A 15 m tall flux tower provided measurements within the SRF site provided measurements of the meteorological conditions at 15-min time intervals (Figure 5b). The meteorological variables used in this study include air temperature, relative humidity and wind speed (4.5 m above the ground). A weighing precipitation gauge (OTT Pluvio) provided measurements of the snowfall rate (q_{sf}) to an open clearing adjacent to the study area shown in Figure 5b. The snowfall rate was corrected for undercatch following phase correction by Harder & Pomeroy (2013) and catch efficiency by Macdonald & Pomeroy (2007).

Snow Surveys

Areal snow surveys provided measurements of throughfall over a discrete time interval (Δt_f). Twelve snow surveys (pre and post event pairs) were selected from a total of 39 snow surveys, resulting in six measurements of snow interception efficiency over the stations shown in Figure 5b.



(a)



(b)

Figure 5: Regional map showing location of Fortress Mountain (a) and map of forest plots, flux towers, and survey transects (b) in this study. ¹¹

If a pre event crust layer was present, post event measurements of fresh snow accumulation above the crust layer were interpreted as throughfall over the event. In the absence of a defined crust layer, the difference of pre and post event snow depth to ground was interpreted as event throughfall. An average of 40 snow depth samples were taken for each snow survey with forest structure ranging from canopy clearing to dense canopy (Figure 5b). A 1000 cm³ snow density wedge sampler manufactured by snowmetrics (<https://snowmetrics.com/shop/rip-1-cutter-1000-cc/>) was used to measure the density of the fresh snow layer.

Lysimeter Data

Three subcanopy lysimeters (e.g., Figure 6a) provided fifteen minute interval measurements of throughfall plus unloading (instrument locations are shown in Figure 5b). For select events where ablative processes, $q_{unld}(L)$, q_{drip} and q_{wind}^{veg} could be considered negligible, the subcanopy lysimeters were inferred to provide measurements of throughfall. Timelapse imagery, a weighed tree and in-situ observations were used to ensure ablation of snow intercepted in the canopy or snow on the ground was minimal over each of the selected events.

A weighed tree lysimeter, shown in Figure 6b and Figure 6c, measured the weight of canopy snow load, L_{wt} (kg). A live subalpine fir (*Abies lasiocarpa*) tree was cut and suspended from a load cell at the beginning of the 2022 and 2023 water years which recorded the weight of the tree. The bottom of the tree was sealed to limit some transpiration and to prevent spinning and abrupt impacts of the free-hanging tree, the base of the tree was attached to a support system that allows for vertical movement but limits abrupt horizontal movements. The weight of snow in the canopy was scaled to an areal estimate of canopy snow load (L , kg m⁻²) using manual snow survey measurements (as in Hedstrom & Pomeroy, 1998).

Snow Interception

Throughfall measurements collected form manual snow surveys ($q_{tf} \cdot \Delta t$) and the subcanopy lysimeters (q_{tf}) were used to estimate the amount of snow intercepted in the canopy. During calm snowfall periods Equation 1 was be simplified to estimate the amount of snow intercepted in the canopy:

$$\frac{dL}{dt} = q_{sf} - q_{tf}(L) \quad (3)$$

This method was preferred, compared to measurements from the weighed tree lysimeter, as the subcanopy lysimeters were not influenced by sublimation losses from snow intercepted in the canopy.

Interception efficiency, $\frac{I}{P}$ (-), which is the fraction of snow intercepted over a discrete time interval, Δt was calculated as:

$$\frac{I}{P} = \frac{\Delta L}{\bar{q}_{sf} \Delta t} \quad (4)$$

where ΔL (mm) is the increase in canopy load over a discrete time interval and \bar{q}_{sf} (mm), is the average snowfall rate over Δt .

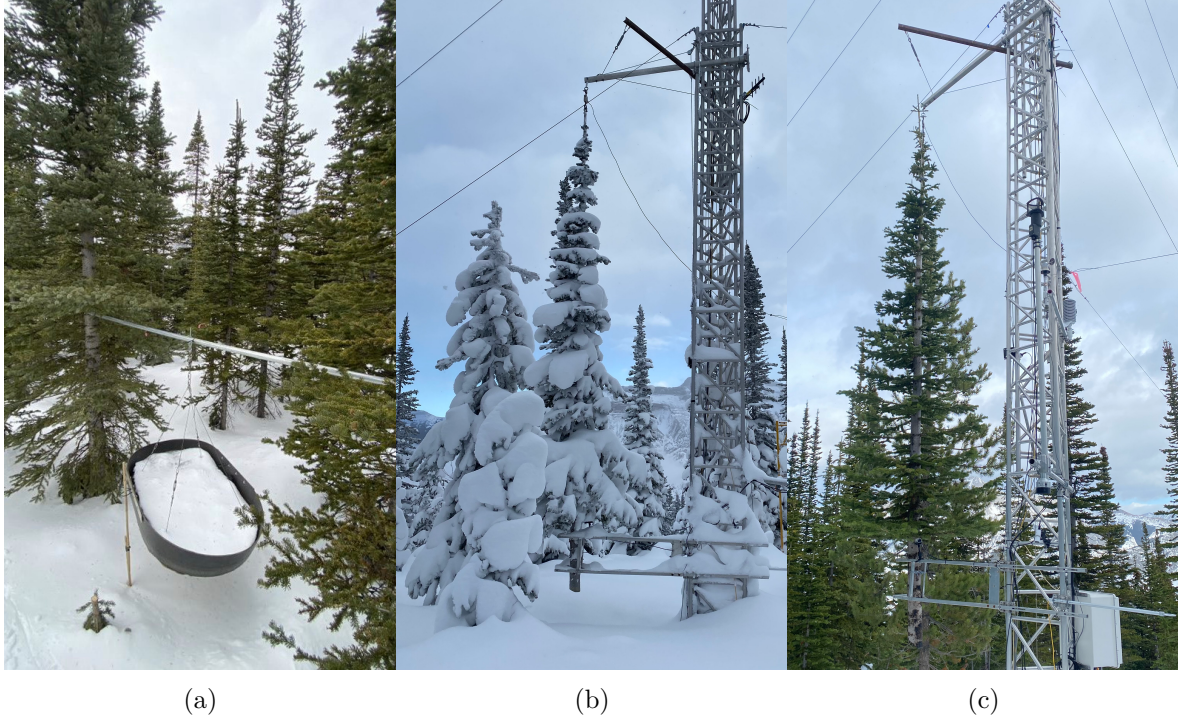


Figure 6: Subcanopy lysimeter (a), weighed tree lysimeter loaded with snow (b) and weighed tree lysimeter bare of snow (c).

Results

The influence of meteorology on snow interception

The meteorological conditions, state of canopy snow load, and interception efficiency was measured across 26 distinct snowfall events. The histograms presented in Figure 7, portray the frequency distribution of 15-minute measurements during periods of snowfall over the 26 snowfall events. The average interception efficiency observed across all periods of snowfall using the subcanopy lysimeters was 0.64 and ranged from 0 to 1. The air temperatures spanned from -25°C to 1°C, with a predominant concentration of observations within the -10°C to 0°C

range. Corresponding wind speed values ranged from 0 to 4.5 m s⁻¹ with a mean of 1.2 m s⁻¹.

The state of canopy storage with event cumulative snowfall was measured using the subcanopy lysimeters and snowfall gauge and is shown in Figure 8a for 26 snowfall events. The interception efficiency was calculated for each of the 26 snowfall events using ?@eq-tbd and is shown in Figure 8b across different event snowfall totals. The subcanopy lysimeters corresponding canopy coverage of 0.73, 0.78 and 0.82. However, looking at the individual events in both panels of Figure 8 higher canopy coverage does not consistently yield higher interception efficiency for events with the same total snowfall. The variation in the rate of change (i.e., 15 minute interception efficiency) between the events at the same location is interpreted to be due to diverse meteorological and antecedent canopy snow load conditions which outweigh the differences in canopy structure between the troughs for most of the events analysed.

The change in interception efficiency was also analysed independently of each snowfall event in Figure 9 by showing the average interception efficiency and corresponding variable over each 15-minute timestep where snowfall was observed. Air temperature and relative humidity was observed to have little influence over interception efficiency measured over the 26 snowfall events (Figure 9, A & B). Wind speed was observed to increase the mean interception efficiency slightly from 0.56 to 0.62 between wind speed bins of 0.25 and 1.25 m s⁻¹ (Figure 9, C). This is thought to be due to an associated increase in canopy contact area as hydrometeor trajectory becomes more horizontal with increasing wind speed. The mean interception efficiency decreases wind speeds above 2 m s⁻¹ to a minimum of 0.48 for the 3.75 m s⁻¹ wind speed bin. The initial canopy snow load had a positive association with interception efficiency as the canopy filled with snow, increasing the mean interception efficiency from 0.57 for snow loads near 0 mm to 0.66 for snow loads around 7 mm. This was followed by a gradual decline in interception efficiency for snow loads greater than 7 mm to a minimum of 0.48 at snow loads above 18 mm (Figure 9, C). Hydrometeor diameter and velocity did not have a strong association with interception efficiency (Figure 9, E & F).

The influence of forest structure on snow interception

Snow interception efficiency observed across the study site after a 24 hour snow accumulation event reveals the influence of forest structure on snow accumulation. The meteorology from this snowfall event, totalling 28.4 mm between lidar flights on March 13th and 14th, is shown in Figure 10. The event was characterised by a transition from low rates of snowfall with near 0°C air temperature and northeasterly winds from 1.5–2 m s⁻¹. Higher rates of snowfall began late afternoon on March 13 and coincided with temperatures around -2.5 °C and predominately southerly winds around 1–2 m s⁻¹. The frequency distribution of lidar measured throughfall is shown in Figure 11. Lidar measured throughfall was used in Equation 3 along with snowfall measurements from the Pluvio Snowfall Gauge to calculate $\frac{\Delta L}{\Delta t}$.

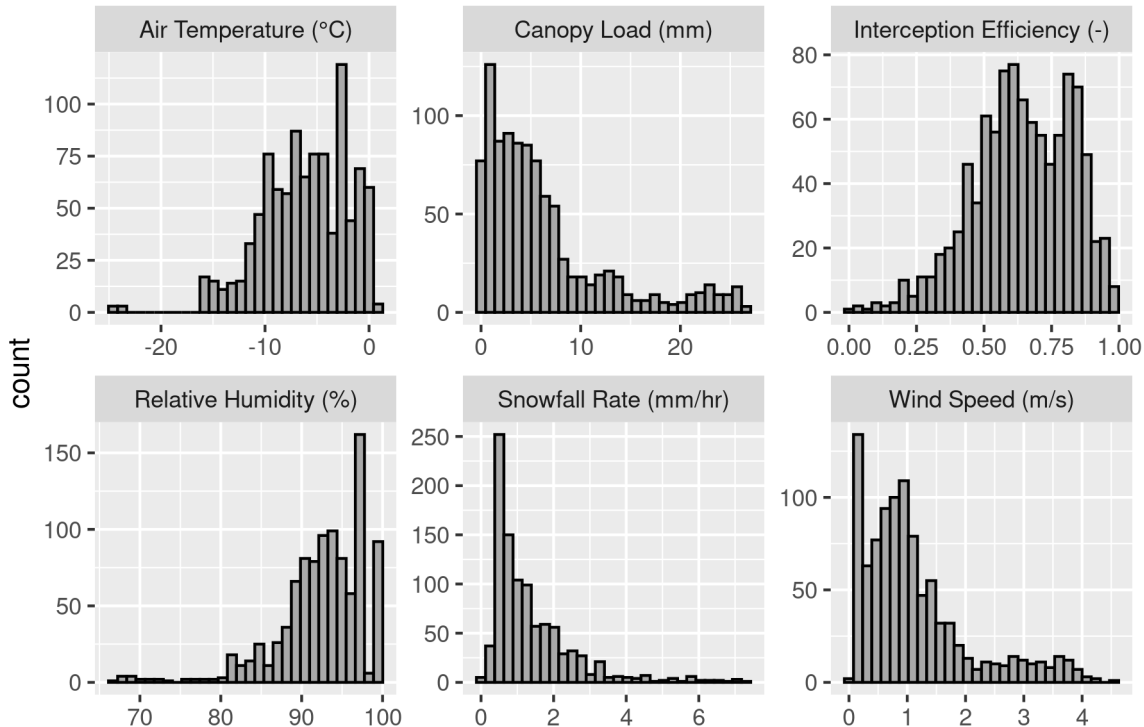


Figure 7: Histograms of meteorological variables and interception variables for 15 minute observations over periods with snowfall over the study period.

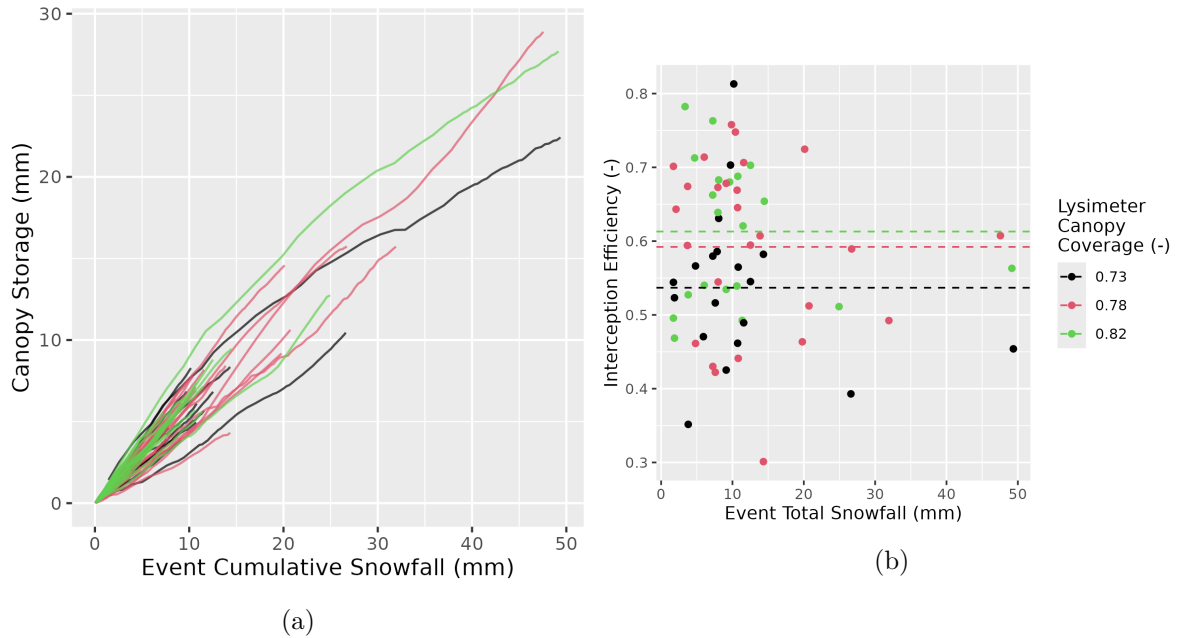


Figure 8: The left panel (a) shows the cumulative canopy snow storage measured using the sub-canopy lysimeters plotted against cumulative event snowfall for 26 snowfall events. The right panel (b) shows event total snowfall versus the average interception efficiency for each event. Snowfall in this plot was measured using the snowfall gauge at Powerline Station.

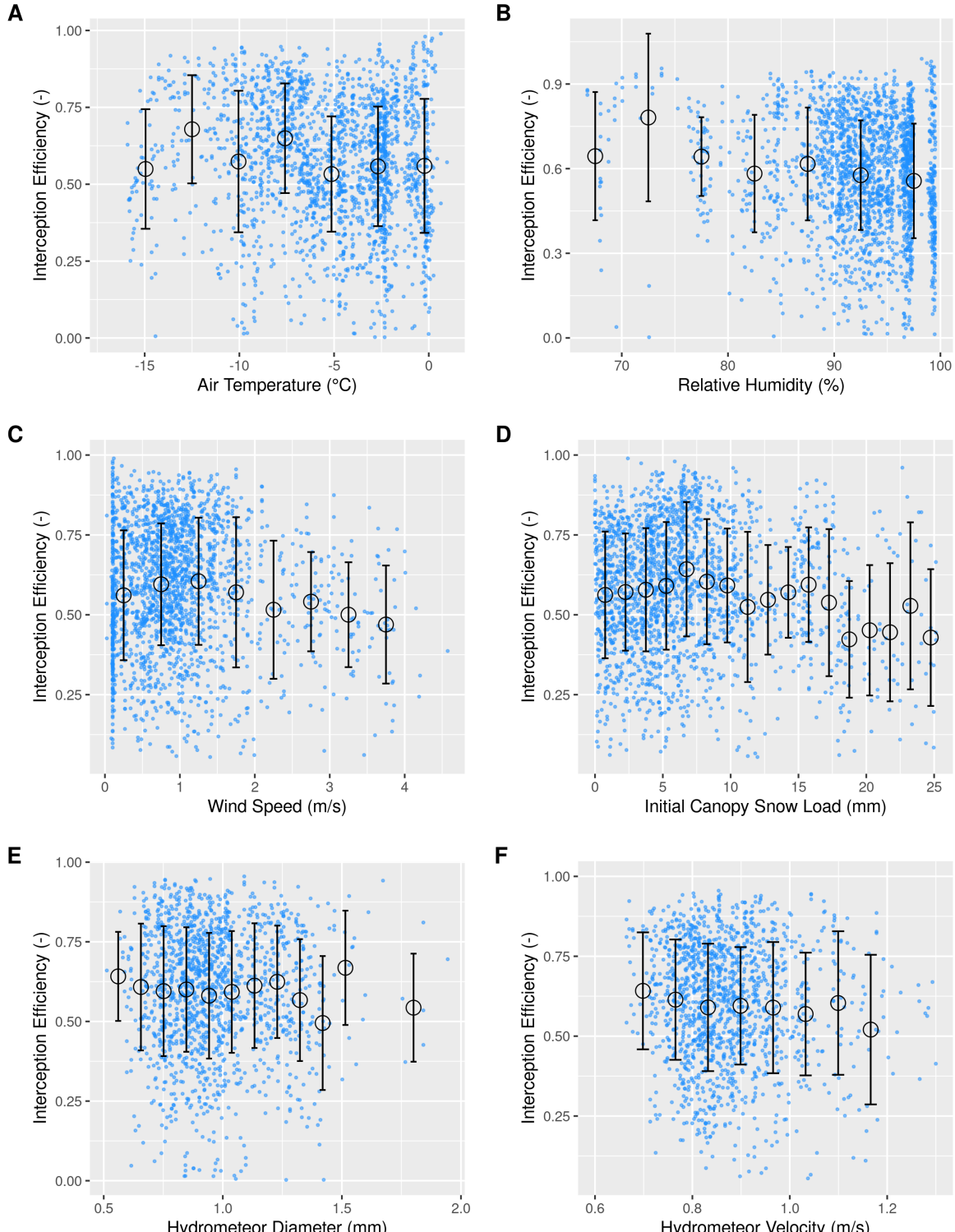


Figure 9: Scatter plots of discrete observations (green) of snow interception efficiency observed at 15 minute intervals using the subcanopy lysimeter and snowfall gauge against and binned data (black). Panels show (A) air temperature, (B) wind speed, (C) initial canopy snow load (the snow load observed at the beginning of the timestep), (E) hydrometeor diameter, (F) hydrometeor velocity. The black open circles show the mean of each bin and the error bars represent the standard deviations. The data were filtered to include observations with a snowfall rate $> 0 \text{ mm/hr}^{-1}$ and a snowfall rate $>$ the subcanopy lysimeter throughfall rate to minimize observations with unloading. Periods of unloading and melt were also removed through careful analysis of the weighed tree, subcanopy lysimeters, and timelapse imagery.

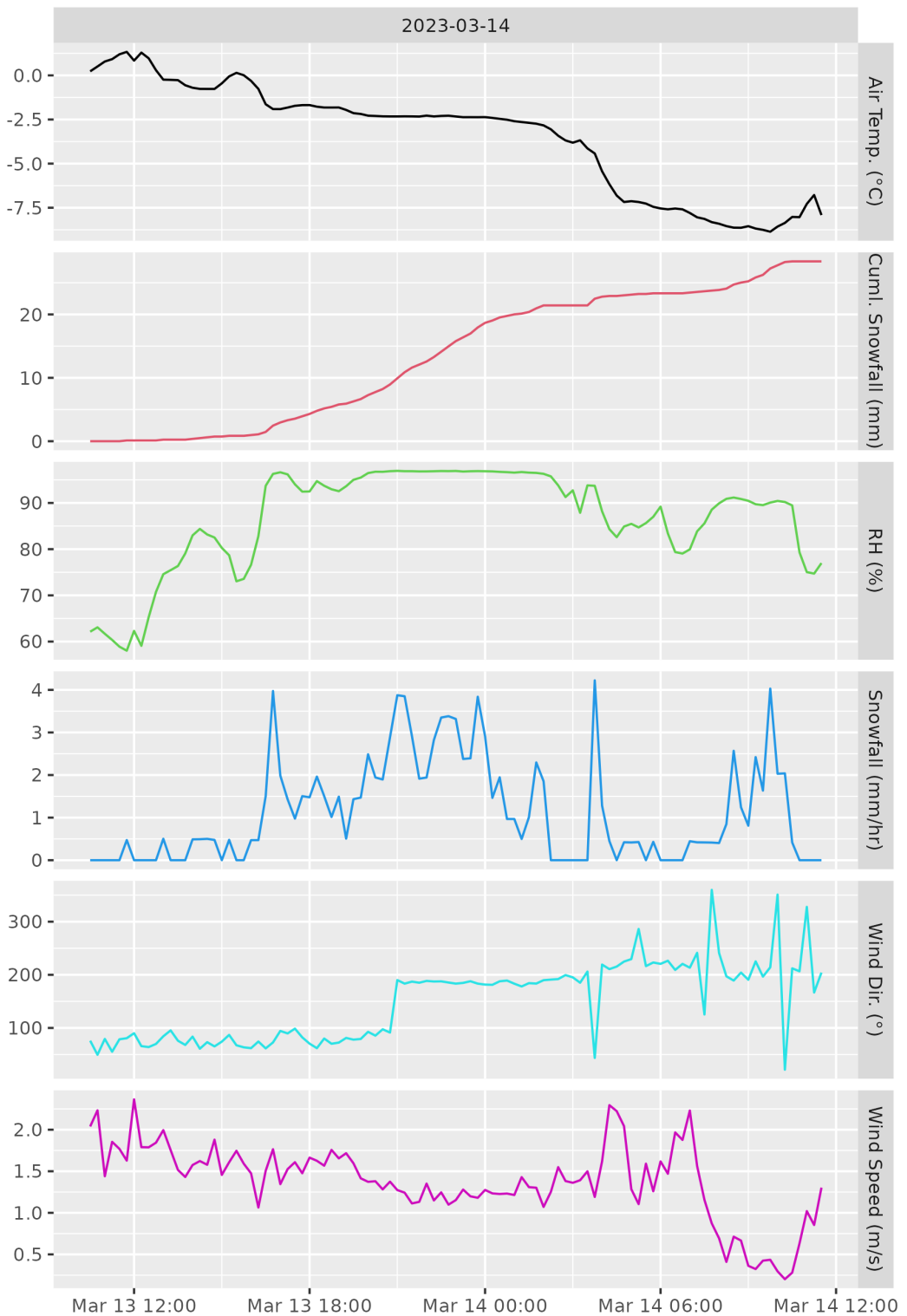


Figure 10: Meteorological conditions over the duration of the March 13, 2023 snowfall event.

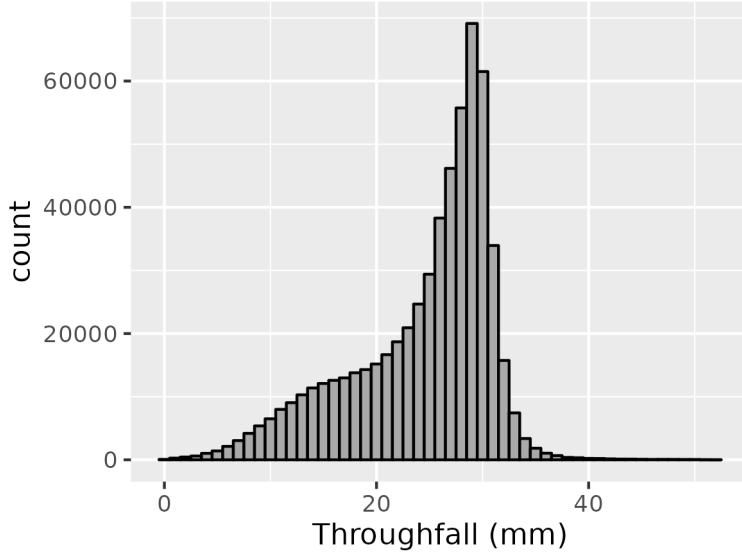


Figure 11: Frequency distribution of lidar measured throughfall over the 24 hour snowfall event between March 13 and 14th, 2023.

The spatial distribution in I/P across the study site, calculated using Equation 4 and ΔL from lidar measurements and Δsf from the Pluvio snowfall gauge is shown in Figure 12. Greater I/P is observed on the north (lee) side of individual trees which is inferred to be due to the predominately southerly winds observed over this event. This effect is more apparent on the southwest of the study site compared to north and eastern locations within the study site.

To determine how forest structure was associated with interception efficiency over the March 13-14 snowfall event, each portion of the hemisphere at each grid location was considered. The Spearman's Correlation Coefficient calculated between the single raster grid of I/P and multiple canopy contact number at a given portion of the hemisphere (azimuth [0, 1, ..., 359], zenith angle [0, 1, ..., 90]) is shown in Figure 13. The hemisphere plots show that the number of canopy contacts along rays to the south with a zenith angle of 0-30° had the highest correlation with interception efficiency. This suggests that hydrometeors had trajectory angles that were predominately non vertical over the duration of this event. This aligns with the meterology of the event which had a median wind speed of 1.4 m s^{-1} , median wind direction of 183° , median hydrometeor velocity of 0.9 m s^{-1} resulted in a predicted median hydrometeor trajectory of -33° from a horizontal plane.

For a more closed canopy (Figure 13a, PWL_E) with a canopy coverage of 0.37, the correlation between interception efficiency and mean contact number across the hemisphere, aggregated for each grid cell, within each plot, shows that the highest Spearman's R correlation is observed between zenith angles of 15-30° and azimuth of 180-190° South. For more open canopy (Figure 13b, FSR_S) with a canopy coverage of 0.2 the peak correlation slightly lower and

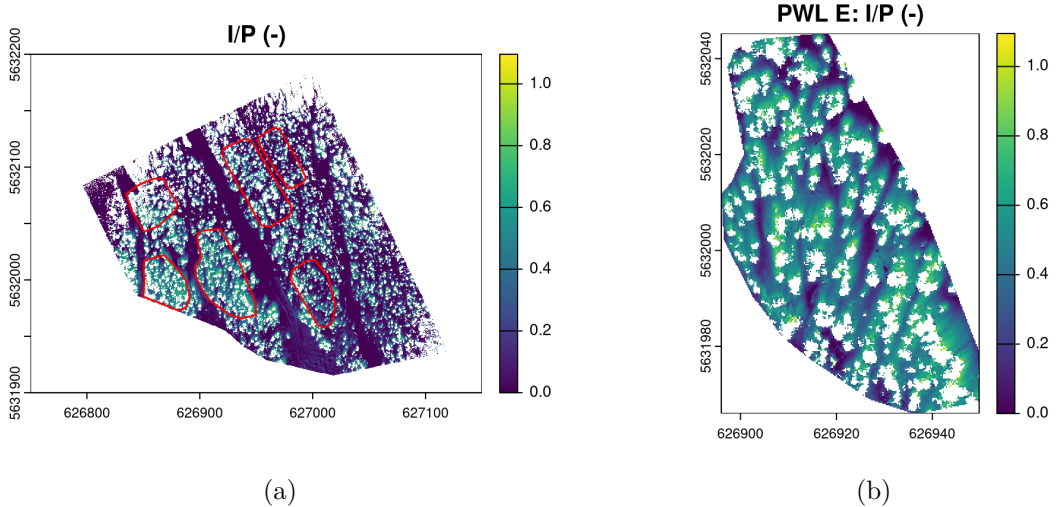


Figure 12: Interception efficiency calculated over a 24 hr snowfall event from March 13, 2023 to March 14, 2024 at a 25 cm resolution. The entire extent of the lidar transect is shown on the left (a) and a close up of PWL_E on the right (b). White areas are 25 cm grids that did not have any lidar returns and thus, no throughfall measurement for the I/P calculation.

not as localised, while still highest around zenith angles of 15-30° and azimuth angles of 180-190°South.

Combined Effects of Meteorology and Forest Structure

The mean canopy coverage across the hemisphere for each forest plot, estimated as a function of the estimated number of canopy contacts along a ray show an increase in canopy coverage with increasing horizontal hydrometeor trajectory Figure 14b. Forest plot PWL_SW which has a more closed canopy has 0.4 (-) fractional closed canopy at near vertical trajectories (near -90°) and increases at a slower rate at higher trajectories above -50° compared to sparser canopies like FSR_S which has a lower canopy coverage of 0.2 (-) from nadir and increase in canopy coverage at a higher rate compared to PWL_SW. All forest plots approach completely closed canopies at for horizontal (0°) trajectories. Since hydrometeor trajectory may be estimated as a function of wind speed, assuming constant hydrometeor terminal fall velocity and horizontal velocity equal to wind speed, ?@fig-ws-cc shows canopy coverage as a function of wind speed. Most of the increase in canopy coverage as a result of horizontal hydrometeor trajectories occurs between wind speeds of 0 and 2 m s⁻¹. However, this relationship does not consider the turbulent windflow patterns that exist within and above the canopy.

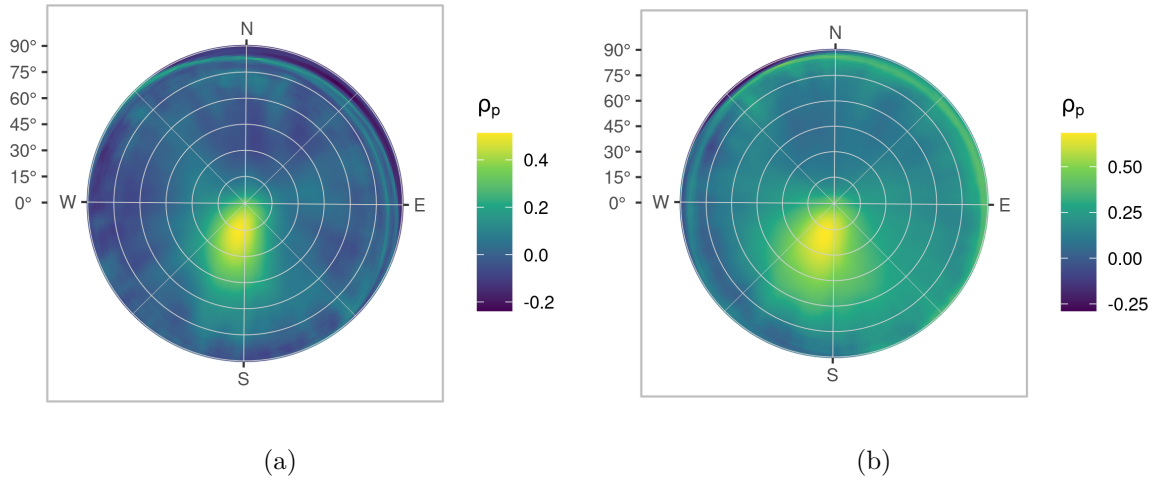


Figure 13: Spearman’s Correlation Coefficient between rasters of interception efficiency and canopy contact number (25 cm resolution) across the study site for different portions of the hemisphere (azimuth $[0, 1, \dots, 359]$, zenith angle $[0, 1, \dots, 90]$).

Discussion

- Forest structure is the primary control in determining the fraction of snowfall intercepted at a given location. A low range in interception efficiency was observed across events with varying snowfall, air temperature, relative humidity, hydrometeor diameter and hydrometeor velocity.
- The largest meteorological influence on interception efficiency observed at the same location across different events was due to wind speed which appeared to increase interception efficiency by almost 10%, while later decreasing I/P due to unloading. Initial canopy snow load had the largest influence on interception efficiency with a 20% change detected between peak snow loads of over 20 mm (low interception efficiency) and optimal snow loads of near 7 mm (high interception efficiency).
- Empirical evidence to support the theory of increased in canopy contact area with increased wind speed (Hedstrom & Pomeroy, 1998) has not been provided in the literature. The snow survey measurements conducted here corroborated with this theory, showing that events with high wind resulted in an increase in interception efficiency at sparse canopy locations. High frequency measurements by the subcanopy lysimeters also showed a slight increase in interception efficiency with increasing wind speed, but at peak wind speeds interception efficiency decreased due to unloading.
- Existing theory suggests either a positive (Storck et al., 2002) or negative (Hedstrom & Pomeroy, 1998) association of air temperature with the maximum canopy storage (Figure 2). The findings presented in this study deviate from the relationships outlined

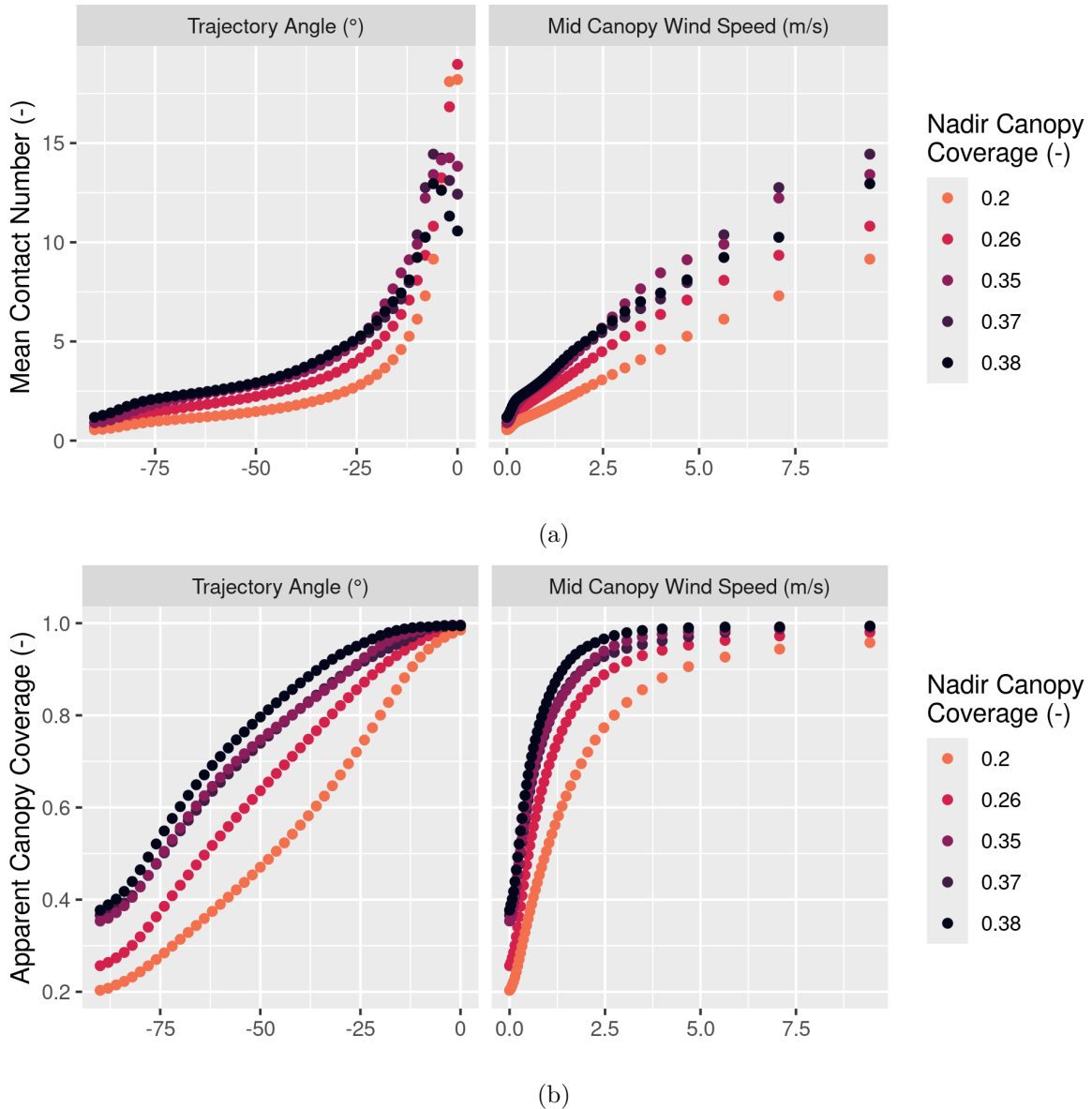


Figure 14: Scatter plots showing the association of (a) hydrometeor trajectory angle and wind speed with mean contact number and (b) hydrometeor trajectory angle and wind speed with apparent canopy coverage calculated as a function of mean contact number. The dots represent the mean mean contact number (a) OR mean canopy coverage (b) across all azimuth angles of the the hemisphere $[0, 1, \dots, 359]$ for a each zenith angle $[0, 1, \dots, 90]$ at each forest plot. The colour of the dot represents the mean canopy coverage of each forest plot from nadir. Trajectory angle is calculated as zenith angle - 90° .

in Hedstrom & Pomeroy (1998) and Storck et al. (2002) concerning the association between air temperature and L_{max} . Specifically, the findings suggest an absence of relationship between air temperature and interception efficiency. The increase in canopy storage with snowfall also did not show any dependence on air temperature or a plateau in storage suggesting the maximum canopy storage value may not have been reached and is likely greater than 25 mm.

- Satterlund & Haupt (1967) showed that interception efficiency increases as the canopy fills with snow bridging gaps in the canopy, while later declining due to branch bending and decreased canopy coverage and increased unloading. Hedstrom & Pomeroy (1998) and Storck et al. (2002) did not observe this initial increase. Observations from the subcanopy lysimeters here showed some evidence for an initial increase in interception efficiency with increasing canopy snow load followed by a decline in interception efficiency likely due to unloading or reduced canopy coverage. The decline in interception efficiency at high canopy snow loads was at rate much slower than has been observed by previous studies (Hedstrom & Pomeroy, 1998; Moeser et al., 2015; Satterlund & Haupt, 1967). At higher canopy snow loads, several studies suggest interception efficiency declines (Hedstrom & Pomeroy, 1998; Moeser et al., 2015; Satterlund & Haupt, 1967), based on the premise of reduced canopy coverage due and catch efficiency to branch bending. However, the strong exponential decline in the interception efficiency observed with increasing event snowfall shown in Figure 1 may be a result of increased unloading rates as branches bend down. The long duration of snowfall events included in Hedstrom & Pomeroy (1998) also increase the likely hood of unloading. This potential inclusion of unloading within the interception parameterizations provided in (Hedstrom & Pomeroy, 1998; Moeser et al., 2015; Satterlund & Haupt, 1967) may lead to double counting of unloading when combined with an additional unloading parameterization as in (Hedstrom & Pomeroy, 1998). However, if interception efficiency is known to decline due to an associated decrease in canopy coverage from branch bending it may be appropriate to have some decline in interception efficiency at higher canopy loads while also having a separate parameterization to increase unloading with canopy snow load.
- Little increase in hydrometeor velocity was observed with increaseing wind speed which supported the use of a constant terminal fall velocity in Equation 2. The increase in velocity above 2 m/s may be due to smaller diameter hydrometeors associated with convective storm activity.

Conclusions

- The forest structure is the main factor in governing the fraction of intercepted snowfall at a particular site, with meteorological conditions contributing less to variability.
- Forest structure metrics calculated using high zenith angles better described the variability in interception efficiency in this windswept subalpine forest.

- Interception efficiency increased with increasing canopy coverage and LAI. However, the strength of this association was reduced at higher wind speeds.
- High wind speeds increased interception efficiency due to an associated increase in canopy contact area for sparsely forested locations, while later decreasing intercepted load due to increased snow unloading.
- No influence of air temperature on interception efficiency or maximum canopy storage was observed.
- Interception efficiency increased slightly as the canopy filled with snow and declined later at higher loads.
- Unloading increased with increasing canopy storage.
- The maximum canopy storage capacity for this study site is likely higher than was observed here.

References

- Andreadis, K. M., Storck, P., & Lettenmaier, D. P. (2009). Modeling snow accumulation and ablation processes in forested environments. *Water Resources Research*, 45(5), 1–33. <https://doi.org/10.1029/2008WR007042>
- Chen, J. M., Rich, P. M., Gower, S. T., Norman, J. M., & Plummer, S. (1997). Leaf area index of boreal forests: Theory, techniques, and measurements. *Journal of Geophysical Research Atmospheres*, 102(24), 29429–29443. <https://doi.org/10.1029/97jd01107>
- Cionco, R. M. (1965). A Mathematical Model for Air Flow in a Vegetative Canopy. *Journal of Applied Meteorology* (1962), 4(4), 517–522.
- Cionco, R. M. (1972). A wind-profile index for canopy flow. *Boundary-Layer Meteorology*, 3(2), 255–263. <https://doi.org/10.1007/BF02033923>
- Clark, M. P., Nijssen, B., Lundquist, J. D., Kavetski, D., Rupp, D. E., Woods, R. A., Freer, J. E., Gutmann, E. D., Wood, A. W., Brekke, L. D., Arnold, J. R., Gochis, D. J., & Rasmussen, R. M. (2015). A unified approach for process-based hydrologic modeling: 1. Modeling concept. *Water Resources Research*, 51(4), 2498–2514. <https://doi.org/https://doi.org/10.1002/2015WR017198>
- Ellis, C. R., Pomeroy, J. W., Brown, T., & MacDonald, J. (2010). Simulation of snow accumulation and melt in needleleaf forest environments. *Hydrology and Earth System Sciences*, 14(6), 925–940. <https://doi.org/10.5194/hess-14-925-2010>
- Ellis, C. R., Pomeroy, J. W., & Link, T. E. (2013). Modeling increases in snowmelt yield and desynchronization resulting from forest gap-thinning treatments in a northern mountain headwater basin. *Water Resources Research*, 49(2), 936–949. <https://doi.org/10.1002/wrcr.20089>
- Essery, R., & Pomeroy, J. W. (2004). Vegetation and topographic control of wind-blown snow distributions in distributed and aggregated simulations for an arctic tundra basin. *Journal of Hydrometeorology*, 5(5), 735–744. [https://doi.org/10.1175/1525-7541\(2004\)005%3C0735:VATCOW%3E2.0.CO;2](https://doi.org/10.1175/1525-7541(2004)005%3C0735:VATCOW%3E2.0.CO;2)
- Essery, R., Pomeroy, J. W., Parviainen, J., & Storck, P. (2003). Sublimation of snow from coniferous forests in a climate model. *Journal of Climate*, 16(11), 1855–1864. [https://doi.org/10.1175/1520-0442\(2003\)016%3C1855:SOSFCF%3E2.0.CO;2](https://doi.org/10.1175/1520-0442(2003)016%3C1855:SOSFCF%3E2.0.CO;2)
- Gelfan, A. N., Pomeroy, J. W., & Kuchment, L. S. (2004). Modeling forest cover influences on snow accumulation, sublimation, and melt. *Journal of Hydrometeorology*, 5(5), 785–803. [https://doi.org/10.1175/1525-7541\(2004\)005%3C0785:MFCIOS%3E2.0.CO;2](https://doi.org/10.1175/1525-7541(2004)005%3C0785:MFCIOS%3E2.0.CO;2)
- Harder, P., & Pomeroy, J. W. (2013). Estimating precipitation phase using a psychrometric energy balance method. *Hydrological Processes*, 27(13), 1901–1914.
- Hedstrom, N. R., & Pomeroy, J. W. (1998). Measurements and modelling of snow interception in the boreal forest. *Hydrological Processes*, 12(10-11), 1611–1625. [https://doi.org/10.1002/\(SICI\)1099-1085\(199808/09\)12:10/11%3C1611::AID-HYP684%3E3.0.CO;2-4](https://doi.org/10.1002/(SICI)1099-1085(199808/09)12:10/11%3C1611::AID-HYP684%3E3.0.CO;2-4)
- Helbig, N., Moeser, D., Teich, M., Vincent, L., Lejeune, Y., Sicart, J. E. J.-E. J. E., & Monnet, J. M. J.-M. (2020). Snow processes in mountain forests: interception modeling for coarse-scale applications. *Hydrology and Earth System Sciences*, 24(5), 2545–2560.

<https://doi.org/10.5194/hess-24-2545-2020>

- Katsushima, T., Kato, A., Aiura, H., Nanko, K., Suzuki, S., Takeuchi, Y., & Murakami, S. (2023). Modelling of snow interception on a Japanese cedar canopy based on weighing tree experiment in a warm winter region. *Hydrological Processes*, 37(6), 1–16. <https://doi.org/10.1002/hyp.14922>
- Krinner, G., Derksen, C., Essery, R., Flanner, M., Hagemann, S., Clark, M. P., Hall, A., Rott, H., Brutel-Vuilmet, C., Kim, H., Ménard, C. B., Mudryk, L., Thackeray, C., Wang, L., Arduini, G., Balsamo, G., Bartlett, P., Boike, J., Boone, A., ... Zhu, D. (2018). ESM-SnowMIP: Assessing snow models and quantifying snow-related climate feedbacks. *Geoscientific Model Development*, 11(12), 5027–5049. <https://doi.org/10.5194/gmd-11-5027-2018>
- Langs, L. E., Petrone, R. M., & Pomeroy, J. W. (2020). A $\delta^{18}\text{O}$ and $\delta^2\text{H}$ stable water isotope analysis of subalpine forest water sources under seasonal and hydrological stress in the Canadian Rocky Mountains. *Hydrological Processes*, 34(26), 5642–5658. <https://doi.org/10.1002/hyp.13986>
- Lumbrazo, C., Bennett, A., Currier, W. R., Nijssen, B., & Lundquist, J. (2022). Evaluating Multiple Canopy-Snow Unloading Parameterizations in SUMMA With Time-Lapse Photography Characterized by Citizen Scientists. *Water Resources Research*, 58(6), 1–22. <https://doi.org/10.1029/2021WR030852>
- Lundquist, J. D., Dickerson-Lange, S., Gutmann, E., Jonas, T., Lumbrazo, C., & Reynolds, D. (2021). Snow interception modelling: Isolated observations have led to many land surface models lacking appropriate temperature sensitivities. *Hydrological Processes*, 35(7), 1–20. <https://doi.org/10.1002/hyp.14274>
- Macdonald, J., & Pomeroy, J. W. (2007). Gauge Undercatch of Two Common Snowfall Gauges in a Prairie Environment. *Proceedings of the 64th Eastern Snow Conference, St. John's, Canada.*, 1974, 119–126.
- Moeser, D., Stähli, M., & Jonas, T. (2015). Improved snow interception modeling using canopy parameters derived from airborne LiDAR data. *Water Resources Research*, 51(7), 5041–5059.
- Parviainen, J., & Pomeroy, J. W. (2000). Multiple-scale modelling of forest snow sublimation: Initial findings. *Hydrological Processes*, 14(15), 2669–2681. [https://doi.org/10.1002/1099-1085\(20001030\)14:15%3C2669::AID-HYP85%3E3.0.CO;2-Q](https://doi.org/10.1002/1099-1085(20001030)14:15%3C2669::AID-HYP85%3E3.0.CO;2-Q)
- Pomeroy, J. W., Parviainen, J., Hedstrom, N., & Gray, D. M. (1998). Coupled modelling of forest snow interception and sublimation. *Hydrological Processes*, 12(15), 2317–2337. [https://doi.org/10.1002/\(SICI\)1099-1085\(199812\)12:15%3C2317::AID-HYP799%3E3.0.CO;2-X](https://doi.org/10.1002/(SICI)1099-1085(199812)12:15%3C2317::AID-HYP799%3E3.0.CO;2-X)
- Rasouli, K., Pomeroy, J. W., & Whitfield, P. H. (2019). Are the effects of vegetation and soil changes as important as climate change impacts on hydrological processes? *Hydrology and Earth System Sciences*, 23(12), 4933–4954. <https://doi.org/10.5194/hess-23-4933-2019>
- Roesch, A., Wild, M., Gilgen, H., & Ohmura, A. (2001). A new snow cover fraction parameterization for the ECHAM4 GCM. *Climate Dynamics*, 17(12), 933–946. <https://doi.org/10.1007/s003820100153>
- Roth, T. R., & Nolin, A. W. (2019). Characterizing Maritime Snow Canopy Interception in Forested Mountains. *Water Resources Research*, 55(6), 4564–4581. <https://doi.org/10.1029/2018WR024089>

- Rutter, N., Essery, R., Pomeroy, J. W., Altimir, N., Andreadis, K. M., Baker, I., Barr, A., Bartlett, P., Boone, A., Deng, H., Douville, H., Dutra, E., Elder, K., Ellis, C. R., Feng, X., Gelfan, A., Goodbody, A., Gusev, Y., Gustafsson, D., ... Yamazaki, T. (2009). Evaluation of forest snow processes models (SnowMIP2). *Journal of Geophysical Research: Atmospheres*, 114(D6), 10–18. <https://doi.org/10.1029/2008JD011063>
- Satterlund, D. R., & Haupt, H. F. (1967). Snow catch by Conifer Crowns. *Water Resources Research*, 3(4), 1035–1039.
- Staines, J., & Pomeroy, J. W. (2023). Influence of forest canopy structure and wind flow on patterns of sub-canopy snow accumulation in montane needleleaf forests. *Hydrological Processes*, 37(10), 1–19. <https://doi.org/10.1002/hyp.15005>
- Storck, P., Lettenmaier, D. P., & Bolton, S. M. (2002). Measurement of snow interception and canopy effects on snow accumulation and melt in a mountainous maritime climate, Oregon, United States. *Water Resources Research*, 38(11), 1–16. <https://doi.org/10.1029/2002wr001281>
- Zhu, J., Matsuzaki, T., & Gonda, Y. (2001). Wind profiles in a coastal forest of Japanese black pine (*Pinus thunbergii* Parl.) with different thinning intensities. *Journal of Forest Research*, 6(4), 287–296. <https://doi.org/10.1007/BF02762470>